Available online at www.sciencedirect.com
SCIENCE DIRECT
Surface & Coatings Technology 197 (2005) 327–335
SURFACE & COATINGS TECHNOLOGY
www.elsevier.com/locate/surfcoat

Oxidation behavior of Cu–Cr environmental barrier coatings on Cu–8Cr–4Nb

Linus U. Ogbuji*

QSS Inc., MS 106-1 NASA Glenn Research Center, Cleveland, OH 44135, United States

Received 7 April 2004; accepted in revised form 10 January 2005
Available online 31 March 2005

Abstract

Oxidation behavior of some Cu–Cr alloys (with 8.5–25.6 wt.% Cr, in both stand-alone coupons and spray coatings on Cu–8Cr–4Nb) was studied by TGA and cyclic oxidation. Judging by the more stringent cyclic oxidation results, protection of the substrate Cu–8Cr–4Nb was effective for the whole 10-h duration of testing up to 750 °C only for coatings with 21% or higher Cr. Similar protection was exhibited by Cu–17Cr only up to 650 °C, and only for <3 h at 750 °C. In all cases the Cr_2O_3 subscale nucleated discretely (and always under a non-adherent scale of Cu oxides), and passive protection did not start until the nuclei joined into a continuous barrier and parabolic oxidation kinetics set in. The only protection achieved before that stage of Cr_2O_3 coalescence was via sacrificial oxidation of the coating.

Keywords: Cu–Cr coatings; Cu–8Cr–4Nb substrate; Oxidation behavior; Cr_2O_3 growth

1. Introduction

Cu–Cr compositions are being developed for use as barrier coatings on the combustion chamber liners of reusable space-launch vehicles, among other applications. This application relies on the expectation of a Cr_2O_3 barrier (from Cr oxidation) to protect the coating and substrate liner. Cu–Cr is especially suited to this application because the liners themselves are Cu alloys and a close match can be tailored between the relevant physical and mechanical properties of the coating and liner: ductility, thermal expansion coefficient, thermal conductivity, etc. For those reasons, the current liner in the Space Shuttle main engine is "NARloy-Z", an alloy with the composition Cu–3 wt.% Ag–0.5 wt %Zr; and the leading contender for liner application in the next-generation launch vehicles that will replace the space shuttle fleet is Cu–8Cr–4Nb, a new copper alloy developed at the NASA Glenn Research Center specifically for this application (and hence designated "GRCop-84"). With GRCop-84 as liner, a Cu–Cr coating would provide the best match of thermo-mechanical properties, which implies better adhesion, lower mismatch stresses, less cracking or spallation, and improved performance and longevity.

Though cumulative service lives are short for launch vehicles (because the main engine fires only in short bursts during a mission), the rapid oxidation of Cu alloys at elevated temperatures is a problem in this application. The oxidation of pure Cu has been widely studied in several respects [1–4], including in oxygen partial pressures similar to those used in the present study [5], but there isn't a substantial body of literature on Cu–Cr oxidation, perhaps because there has not been much commercial interest in Cu–Cr alloys, except for "Chrome Copper"—which typically contains ≤1.0 wt.% Cr, the solubility limit of Cr in solid Cu. In contrast, the proposed Cr levels in liner applications range up to 40 wt.%. Fig. 1 shows the Cu–Cr phase diagram [6], from which it is clear that the liner coatings in this study are two-phase alloys the

* Tel.: +1 216 595 9722; fax: +1 216 591 9456.
E-mail address: linus@ogbuji.net.

0257-8972/$ - see front matter © 2005 Elsevier B.V. All rights reserved.
doi:10.1016/j.surfcoat.2005.01.116

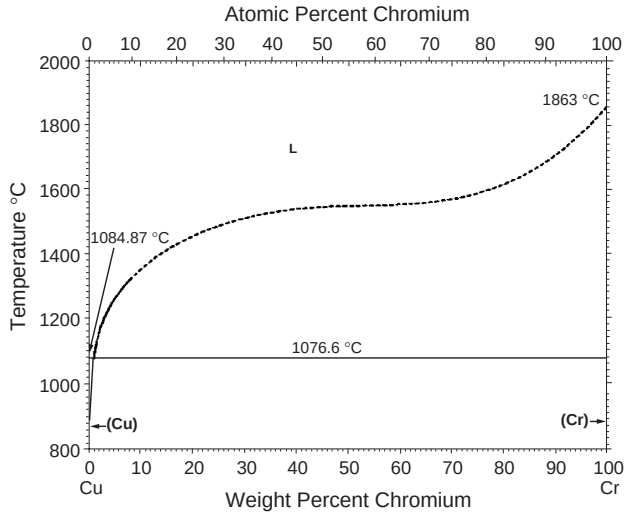

Fig. 1. The Cu–Cr phase diagram: the maximum solubility of Cr in Cu is ≤1%, while Cu is practically insoluble in Cr.

component phases of which are very close to the pure elements, Cu and Cr.

Chiang et al. [7–9] were the first to advocate the use of Cu–Cr coatings to protect Cu alloys in aerospace applications. They found that a protective oxide scale was formed only when Cr content exceeded 30 vol.% (~25.6 wt.%). However, they did not explore the oxidation mechanism of Cu–Cr: in particular, whether it is a true (exclusive) chromia former and why protection is ineffectual below ~25.6% Cr. In air oxidation studies of Cu–Cr alloys with 25–75 wt.% Cr, prepared by a variety of methods, Niu et al. [10] showed that oxidation behavior was strongly dependent on Cr content and how it is distributed, though their melt-cast Cu–Cr was characterized by a coarse dispersion of dendritic Cr in Cu. They found that the amount of Cr_2O_3 formed increased with overall Cr content and temperature, with the growth of a continuous (hence protective) Cr_2O_3 layer occurring over only those areas that were Cr-rich and only at the highest temperature studied (900 °C).

In a related study of the effect of Cr distribution in Cu–Cr [11], the same workers found that the oxide scale which grew on Cu–40 wt.% Cr in 1.0 atm O_2 at 700 and 800 °C was exclusively Cr_2O_3 when the alloy was made by magnetic sputtering to yield untrafine microstructures of ≤10 nm particles. When made by mechanical alloying and comprised of larger (50–300 nm) particles the same alloy grew Cu oxides on top of a Cr_2O_3 sub-layer; and when made by powder metallurgy into coarse microstructures (50–150 μm particles) the oxide layer was a random mixture of Cu and Cr oxides. Thus, in developing Cu–Cr for thrust-cell liner protection via Cr_2O_3 formation, refinement of the Cr distribution may be as important an issue as the choice of Cr content itself, a point that has been explored elsewhere [12].

The oxidation of properly homogenized Cu–Cr alloys may be expected to parallel those of multi-component two-phase alloys in general [13] and chromia-forming intermetallic alloys in particular [14]. Brady et al. have shown that the oxidation rate of a Cr(X) alloy depends on the specific nature of the component X: For instance their oxidation rates are enhanced in some cases by the formation of deleterious Cr–X–O and Cr–X–N–O subscales beneath a Cr_2O_3 scale (with nitrogen coming from the air) [14]. In the present context, the effectiveness of a Cu–Cr coating may be diminished by concomitant formation of copper oxides along with Cr_2O_3, especially if the oxides intergrow in mixed, random clusters in which the most protective constituent oxide does not form a continuous barrier layer.

The aim of this study was to investigate the oxidation of Cu–Cr coatings with a view to determining if and why there is a threshold Cr level for effective Cr_2O_3 protection during launch service, and the possible role of the alloy microstructure in that process.

2. Experimental procedure

Batches of Cu–*x*Cr coatings (*x*=8.5, 17.1, 21.3, and 25.6 wt.% for the different batches) were made by deposition of pre-alloyed Cu–Cr powders of corresponding compositions on substrates and, in some cases, as free-form billets for stand-alone oxidation tests of Cu–Cr. For brevity the compositions are reported here as rounded numbers: 9, 17, 21, and 26Cr. The substrates were coin-shaped Cu–8Cr–4Nb coupons, 1.0 mm thick and 0.75 in. (19 mm) in diameter, polished to 600-grit finish on SiC paper. The Cu–26 wt.% Cr composition was chosen to correspond with the work of Chiang et al., while Cu–9 wt.% Cr was chosen to match the substrate, Cu–8Cr–4Nb; the other two were interpolated at midway points between those two end compositions.

Pre-alloyed Cu–Cr powder was fabricated by Crucible Research Co. of Pittsburgh, PA, by a process of co-atomization of melts from pure (electronic grade) Cu and Cr. Hence, the powder consisted of micro-alloyed Cu–Cr globules. Only the fines (−635 mesh fractions, consisting of <22 μm particles) were used in coating deposition; the coarse fraction was discarded. Inovati Co. of Goleta, CA deposited the coatings, employing their trademark "Kinetic Metallization" (KM) process. In this process, which may be viewed as a variant of the familiar cold-spray process, the particles are entrained in an inert carrier gas (He in this case), accelerated to high subsonic speeds, and trained on the unheated substrate [15]. The high-energy impact cleans and heats the substrate, and flattens the globules as the coating deposit builds up. The powder does not melt, and the inert carrier gas prevents its oxidation. Therefore, KM is especially suited to the deposition of Cu, which is ductile and easily oxidized.

(Before adopting KM for this study, low-pressure plasma spray, LPPS, was tried and found to be unsuitable—because it resulted in high oxygen pick-up and consequent oxidation of the coating around the individual splats.) The coatings, ~7 mils (175 μm) thick on average, were consolidated by the supplier via annealing or HIPing in Ar above 900 °C.

The integrity and consolidation of the coatings were tested by means of both microhardness indentation and the Sebastian Pull Test. The pull test, now standard for evaluating the adhesion of coatings, consists of gluing a stub to the coating and pulling it pneumatically until separation occurs. Failure at the glue is the acceptable result; failure within the coating is undesirable as it indicates poor coating cohesion, and failure at the coating/substrate interface is unacceptable because it indicates poor adhesion.

Oxidation tests were conducted by static and cyclic exposure. Static oxidation was performed in a thermogravimetric analyzer (TGA) through which Ar-buffered UHP O_2 was flowed. The oxidant composition was 2.2% O_2. It corresponds roughly to the reduced oxygen partial pressures expected in liquid-oxygen/liquid-hydrogen ("LH–LOx") rocket engines operating at optimal oxidant-to-fuel (O/F) ratios [16] and is in keeping with our finding that above ~0.25% O_2 at 1.0 atm the oxidation rates of common aerospace Cu alloys is not sensitive to prevailing $p(O_2)$ levels [17]. Cyclic oxidation was performed in lab room air. Static and cyclic oxidation temperatures ranged from 550 to 750 °C and exposure times were 10–20 h—an order of magnitude longer than expected service lifetimes in thrust-cell service. In the TGA tests, sample weight was acquired automatically and continuously; in the cyclic oxidation experiments, the samples were brought out every fifteen minutes, cooled and weighed, and returned to the furnace. Microstructures of exposed coupons were obtained by light microscopy and scanning electron microscopy (SEM) on both the as-exposed surface and polished cross-sections. A JEOL JSM-840A and Hitachi S-4700 HRSEM were used for SEM imaging.

3. Results

Fig. 2 is a plot comparing the TGA weight gain behavior of all the materials at 650 °C: that is, the substrate Cu8Cr4Nb (S) when bare and when coated with each of the four Cu–Cr alloys under investigation. The interval denoted τ at the bottom of the plots indicates the approximate target lifetime of a liner, determined by multiplying the estimated cumulative firing times of a rocket main engine during a mission by the desired number of missions.

Fig. 3(a) presents TGA oxidation kinetics of one of the coating alloys, Cu–21Cr, tested as a stand-alone coupon.

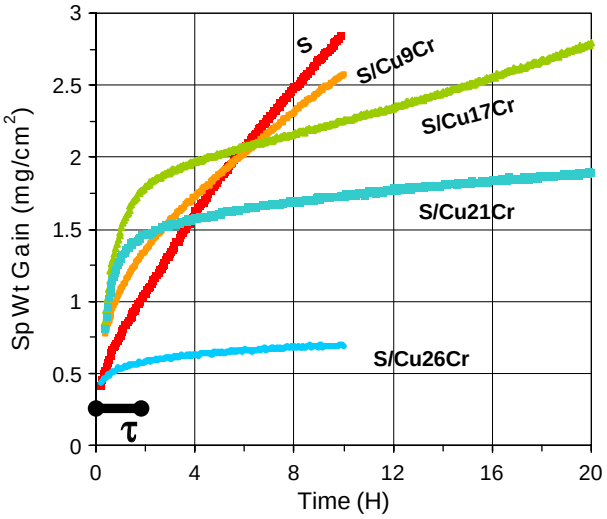

Fig. 2. A comparison of the weight gain rates, at 650 °C in 2.2% O_2 (balance Ar), of the substrate, S (Cu–8Cr–4Nb) alone, and when coated with the various Cu–Cr alloys in this study: the interval denoted τ indicates the approximate service life expected of a liner.

The data is shown as parabolic plots of specific weight gain versus the square root of time for the different temperatures. Results for the other stand-alone alloys are not shown here but were very similar. Oxidation rate accelerated in going from 550 to 750 °C; and transition from transient oxidation to steady-state (which is indicated with dotted vertical strokes) shifts to shorter times with increasing temperature. It is to be noted that there are two different transition events of interest in this study. There is the time it takes for the weight-gain curve of a coating to fall below that of the substrate; that is, the time at which the two curves cross in Fig. 2. The other is the time it takes for the oxidation kinetics of a coating to become parabolic, which is denoted in Fig. 3.

Fig. 3(b) is an Arrhenius plot comparing parabolic rate constants (k_p) determined from these TGA studies of Cu–21Cr and Cu–26Cr, and those for the substrate material and for pure Cu. (The data for Cu–8Cr–4Nb and pure Cu were taken from Ref. [5].) The data for the coating alloys lie considerably below those for the substrate, which suggests that, for prolonged oxidation exposures that last far into the domain of steady-state (parabolic) oxidation, the coatings should provide passive protection for the substrate.

Table 1 summarizes the total weight gains of coated and uncoated Cu–8Cr–4Nb coupons after 20 h in the TGA. Weight gains for the coating alloys in this table were normalized by dividing with the corresponding weight gains for the uncoated substrate. The result is shown as a histogram in Fig. 4, in which the ordinate is specific weight gain of a coated coupon relative to the uncoated substrate when oxidized under the same conditions. On the horizontal axis is the Cr content of the coating under consideration. An ordinate value equal to or greater than 1.0 indicates an ineffective coating, for it means that the coated coupon

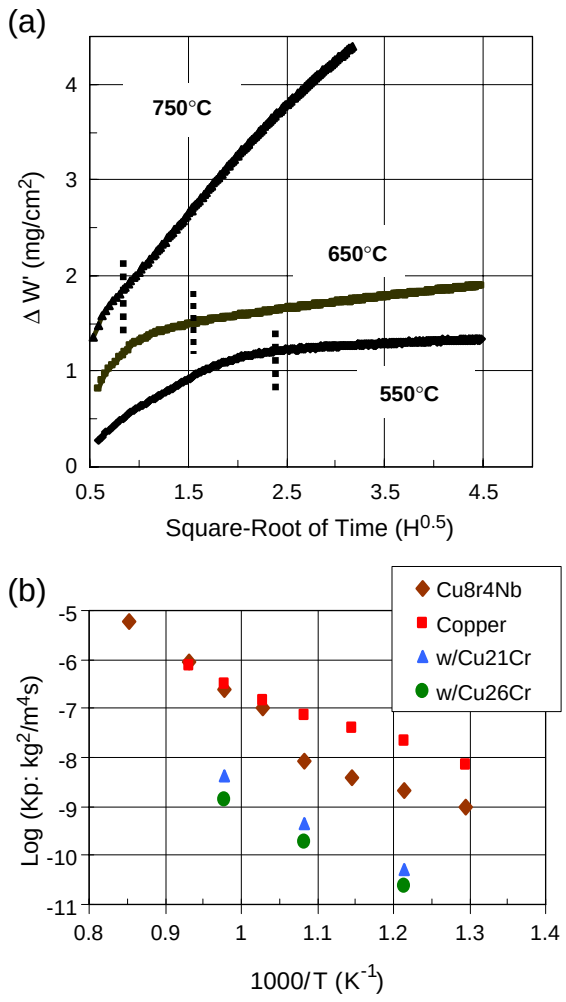

Fig. 3. Oxidation data for Cu–8Cr–4Nb coated with Cu–21Cr and Cu–26Cr and oxidized by TGA at various temperatures: (a) plots for parabolic kinetics, (b) Arrhenius plots of parabolic rate constants.

gained as much or more weight than the bare substrate. Conversely, values of 1.0 or less imply that the coating is protective—and the lower the value the more protective is the coating. This result was used as the basis for preliminary screening of the coating compositions for effectiveness as a coating. It may be seen that all the alloys are protective in static oxidation, except for Cu–9Cr oxidized at 650 °C and above. Predictably, the degree of protection increases with Cr content.

Fig. 5 is an SEM (SE) image of one of the TGA-tested samples sectioned and polished after exposure. The

Table 1
Specific weight gains (mg/cm^2) of coated and uncoated Cu8Cr4Nb coupons during TGA oxidation in 2.2% O_2 at different temperatures

Temperature (°C)	Composition of Cu–Cr Coating on Cu–8Cr–4Nb				
	None	8.5Cr	17.1Cr	21.3Cr	25.6Cr
550	1.72	1.14	0.67	0.61	0.54
650	2.54	2.73	0.83	0.82	0.73
750	7.84	8.26	6.83	4.42	1.95

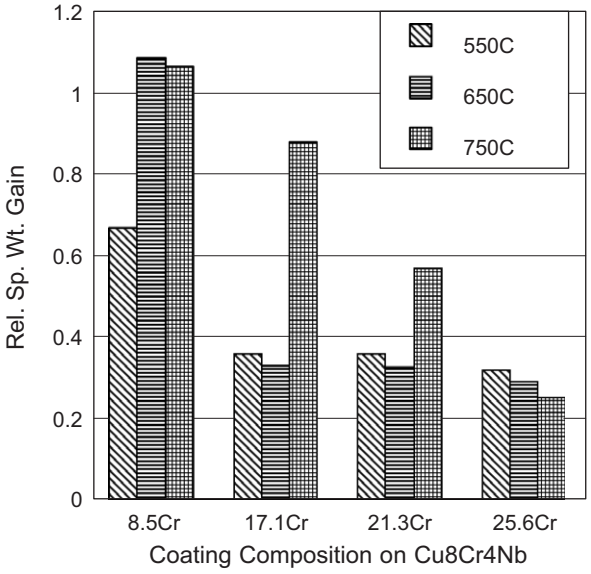

Fig. 4. Normalized specific weight gains for Cu–8Cr–4Nb coated with Cu–Cr compositions and exposed in the TGA for 20 h in 2.2% O_2.

sample, GRCop84 coated with Cu–21Cr, was exposed for 20 h in a TGA at 650 °C. Fig. 5(a) shows the full cross-section, from substrate (S), through coating (C), to oxide. The oxide layer is duplex: The inner oxide layer (IO in the figure) is most likely Cr_2O_3 because EDS and EPMA (electron-probe micro-analyzer) detected only Cr and O in it; and it was adherent to the coating in every case. MO in Fig. 5(a) identifies a middle oxide layer, adherent to the inner oxide, and which had strong Cu and O signals as well as low Cr peaks. It may be a binary Cu–Cr–O oxide (perhaps Cr-containing Cu_2O). For Cu–21Cr and Cu–26Cr the inner oxide layer was always continuous; in Cu–17Cr they were continuous only when oxidation was performed at 750 °C. There was in every case a very thick outer oxide scale which spalled off upon cooling. This outer scale was an order of magnitude thicker than the adherent oxide films in Fig. 5(a), and it was the double strata of Cu_2O (inner layer) and CuO (outer veneer) already identified as the preponderant oxidation product of Cu and its alloys [5,17].

Fig. 5(b) shows the boundary zone between the substrate and coating. The light spots are the fine Cr_2Nb precipitates of the substrate; the dark larger islands are Cr in the coating which agglomerated during consolidation anneal/HIP and subsequent oxidation exposure. Continuity of the Cu matrix across the boundary between substrate and coating and the lack of cracks and/or pores along the same boundary are indicators of excellent adherence of coating to substrate. Fig. 5(c) shows the coating and the oxide layers adherent to it.

Cyclic oxidation tests are considered more rigorous than static oxidation. They are also more definitive because failure of protection is often clearly evidenced in dramatic loss of weight when non-protective oxide

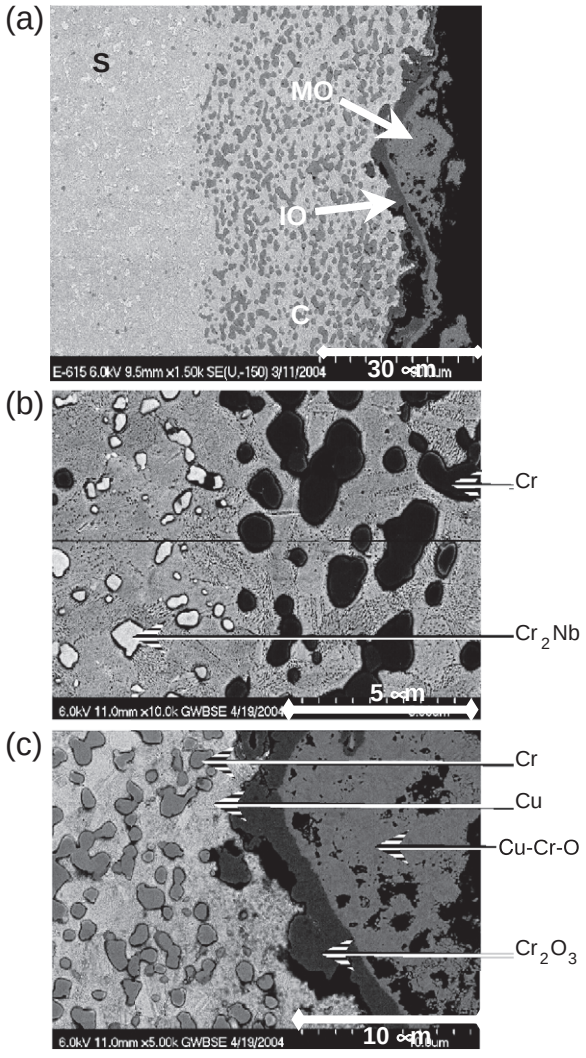

Fig. 5. SEM cross-sections of a coated sample oxidized by TGA for 20 h at 650 °C: (a) full section, showing substrate (left), coating (middle), and oxide (right); (b) the substrate-coating boundary, and (c) the coating-oxide zone.

spalls off [18]. Therefore, those coating compositions which were judged from the foregoing results to have performed well in static oxidation were put to the more rigorous test of cyclic oxidation at 650 and 750 °C. The results are shown in Fig. 6: exposed coupons in Fig. 6(a) and their cyclic oxidation weight changes in Fig. 6(b). The samples and their corresponding weight-change curves are numbered 1, 2, and 3 in both figures. Note that 1 actually includes a total of four curves which are lumped together because they behaved in the same way during exposure.

Hence, the numbers also denote the three categories of weight-change behavior observed in cyclic oxidation. In Type-1 behavior the coated samples exhibited little or no weight change and the sample looked unblemished after the 10-h exposure; at 650 °C and below, all three coatings fell into this category, as did Cu–26Cr up to 750 °C. In Type-2 behavior the samples changed from weight gain to weight loss regimes about half-way through the run and showed evidence of coating breach at the end of the run; Fig. 6 shows that Cu–21Cr had Type-2 behavior at 750 °C and Type-1 behavior at lower temperatures. Type-3 behavior is characterized by rapid initial weight gain, followed by catastrophic weight loss early in the exposure, with the coupon bearing clear signs of coating (and substrate) degradation and loss at the end of the run; Cu–17Cr displayed Type-3 behavior at 750 °C and Type-1 behavior at lower temperatures.

To determine how deeply damage had penetrated in Samples 2 and 3, they were sectioned, polished, and examined by SEM. The images are shown in Fig. 7(a) and (b), respectively. Both of the samples started with the same thickness of coating (~175 μm). At the end of the test the residual thickness of coating left on Sample 2, determined from 8 readings around the coupon) was ~45 μm; that is ~25% of the coating thickness remained intact. In contrast, Sample 3 had lost all its coating and

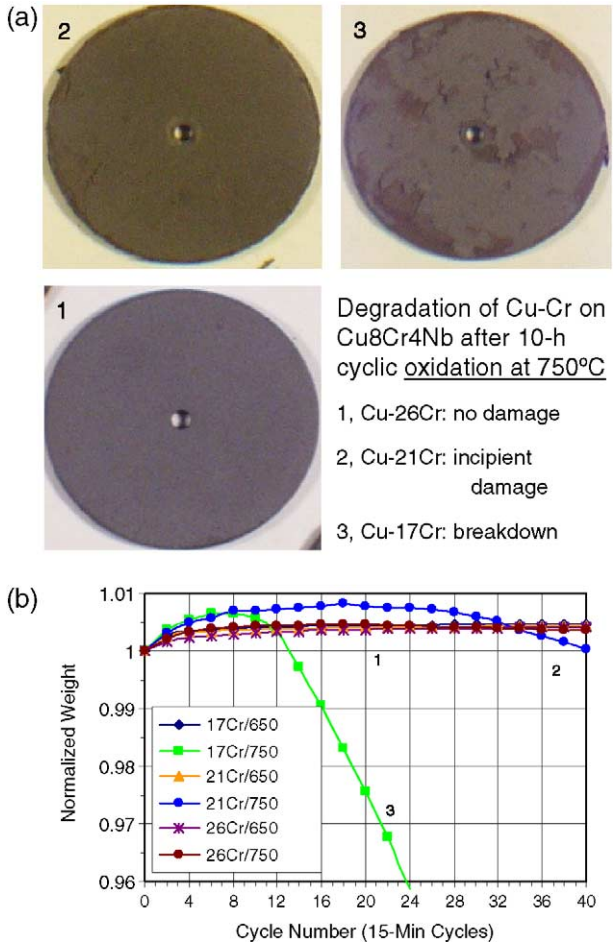

Fig. 6. Weight gains (normalized to initial weights) for three Cu–8Cr–4Nb coupons coated with different Cu–Cr compositions and cyclically oxidized for 10 h at 650 and 750 °C: 1, 2, and 3 refer to three categories of behavior observed.

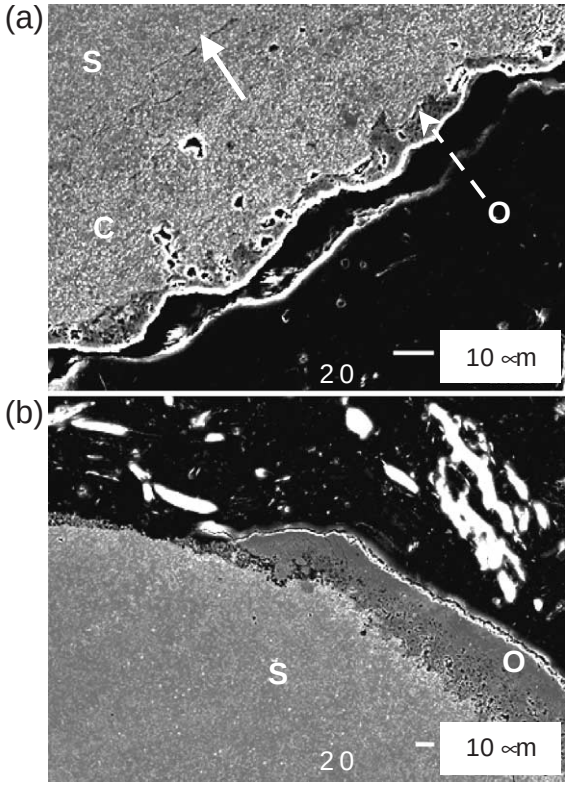

Fig. 7. SEM images from the cross-sections of cyclic oxidation samples following 10-h exposures at 750 °C: (a) Cu–21Cr, (b) Cu–17Cr coatings. S is the Cu–8Cr–4Nb substrate, C the coating, O the oxide scale. The short, solid arrow in (a) denotes the coating/substrate interface.

started oxidizing the substrate: Fig. 7(b) shows the residual oxide scale on Sample 3 interfacing directly with the substrate, S.

Fig. 8 is a pair of SEM cross-sections (BSE mode) from coated coupons oxidized for 20 h at 650 °C. Fig. 8(a) is from the Cu–17Cr coating, while Fig. 8(b) is the same view of the Cu–21Cr coating which we have already seen in Fig. 5. EDS spectra from identified features in both figures are shown alongside the images. The phases in Fig. 8(a) may be recognized through a comparison with those in Fig. 8(b), which were identified in Fig. 5: the phase labeled D is clearly Cr_2O_3, while E is the Cr–Cu–O binary oxide (or Cr-containing Cu_2O) mentioned earlier; the particles of Cr in the coating are also labeled. Phase D (Cr_2O_3) forms a continuous layer in the case of Cu–21Cr but only distinctly separate colonies in the case of Cu–17Cr.

4. Discussion

Results have been presented elsewhere concerning the integrity of the coatings [12]. The salient points are: (1) Indentation and Pull tests showed that the coatings exhibited excellent cohesion and adhesion, (2) porosity was minimal, and (3) there was no evidence of surface-connected cracks or pores at the substrate-coating interface. These observations are also evident in Fig. 5, which shows a seamless transition from substrate to coating. Consequently, any lack of protection observed in this study can only be intrinsic rather than due to defects in the coating. The intrinsic oxidation behavior, vis-à-vis protection, will now be discussed.

The main questions addressed in this study are whether Cu–Cr alloys can protect a Cu–8Cr–4Nb substrate of a thruster liner, and whether the protection can be effective when the Cr content is kept low to prevent significant decrease of coating ductility and conductivity. These questions were explored by means of static (TGA) and cyclic oxidation schemes in this study. The most severe oxidation-related mode of liner degradation is, of course, blanching and not static or cyclic oxidation [5,16], but it has been determined that blanching (simulated with oxidation–reduction cycling) is not an effective discriminant for optimum Cr level in this system because all Cu–Cr compositions, from 9 wt.% to 26 wt.% Cr were uniformly resistant to oxidation–reduction cycling [19]. So we have to rely on static and, especially, cyclic oxidation tests to provide some answers.

The first level of answer comes from the k_p values shown in Fig. 3(b), which shows that Cu–Cr alloys, typified in the figure by Cu–17Cr and Cu–26Cr, can protect the substrate in oxidation exposures that are prolonged enough for passive oxidation to set in. Just as k_p values for the oxidation of Cu8Cr4Nb, the substrate in this study, are generally an order of magnitude lower than for Cu [5], Fig. 3(b) shows that the values for the Cu–Cr alloys in this study are even lower than for the substrate by another order of magnitude or more. Hence, for long-term oxidation these Cu–Cr alloys resist oxidation even more than the substrate and, therefore, do have the potential to protect the substrate. By considering shorter oxidation times (closer to expected liner life) and quantifying weight gains, a more discriminating answer emerges: A Cu–9Cr alloy gains more weight than the substrate and so would not be effective as a coating; but the other compositions might be effective because they showed specific weight gains less than 1.0 relative to the substrate (Fig. 4).

As expected, the cyclic oxidation test results provide even better discrimination between the alloy compositions. Effective protection in cyclic oxidation is indicated when a sample stays in the weight-gain regime all through the exposure, as in the samples and test conditions labeled Type-1 in Fig. 6. Type-2 is also acceptable, being borderline protective since the sample does not go into catastrophic weight-loss (Type-3) during the test duration. This figure shows that, for expected liner life under 10 h, all the Cu–Cr compositions are protective for exposure at or below 650 °C, and at 750 °C only Cu–17Cr failed the test. And the failure was drastic: After a dozen cycles or so this sample entered the terminal regime of linear weight loss characteristic of irrecoverable damage [18], and at the end of the test it had lost 10% of its starting weight.

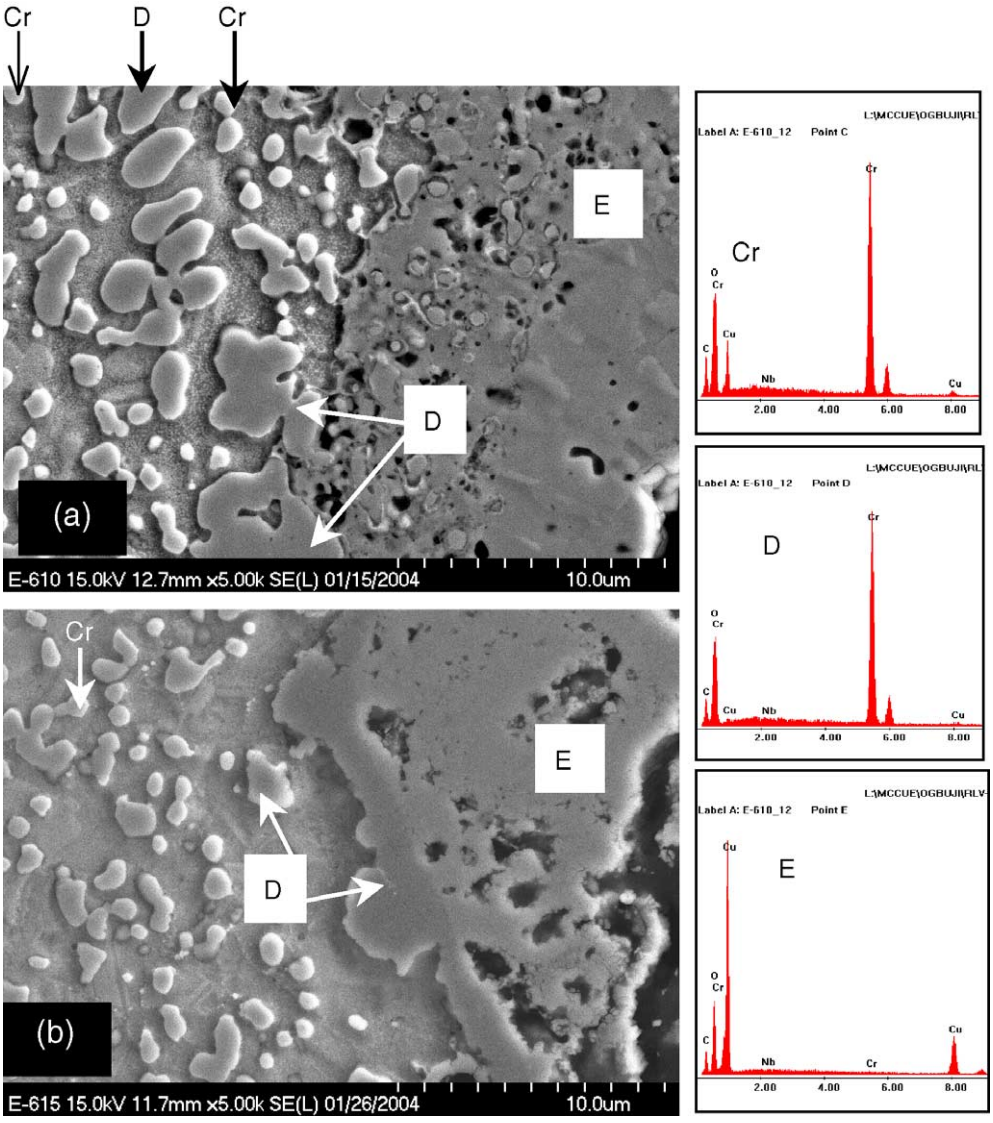

Fig. 8. SEM cross sections from Cu–8Cr–4Nb coated with (a) Cu–21Cr and (b) Cu–17Cr, oxidized in TGA for 20 h at 650 °C. Cr_2O_3 occurs in (a) as a continuous film and in (b) as discrete particles not yet coalesced into a barrier.

Fig. 6 also shows that the judgment as to whether or not a coating passes the test at the given temperature depends on the expected/desired liner life: If only a ~3 h liner life (corresponding to 12 cycles in this study) is envisioned, then all the alloys performed satisfactorily. Note also that the less protective the coating was, the higher the maximum weight it attained before weight loss set in; the maximum weight reached reflects the total oxidation weight gain, while the steepness of the linear terminal region reflects the rate of oxide loss from spallation [18]. Weight changes in Fig. 6(b) provide an indication (while Fig. 7 gives pictorial confirmation) that the failure of Sample 3 is associated with total consumption of coating and consequent oxidation of the substrate. This sample lost over 10% of its weight in the experiment, but the ~95 μm coating on each side of the substrate constitutes <10% of the thickness and an even smaller percentage of the sample weight; therefore, Sample 3 must have lost all its coating to oxidation before the end of the experiment.

In sum, these static and cyclic oxidation results establish an inverse relation between the rate of coating consumption by oxidation on one hand, and the concentration of Cr in a coating. Coatings with higher Cr levels are more protective because they are consumed more slowly.

A closer look at the TGA results gives an interesting insight into the kind of protection that may be provided by these coating alloys. Fig. 2 underscores two unique aspects of the problem in liner application revealed by this study. The first is that the desired liner service life, τ, is exceeded before the coating weight-gain curves bend over at the knees signaling transition to parabolic kinetics; therefore, oxidation issues in this system relate to the transient or initial stage of oxidation rather than to the "mature" stage of steady-state oxidation.

The second point is that during the early stage of oxidation the uncoated substrate, S, gains *less* weight than the coated samples (with the sole exception of Cu–26Cr). This has an interesting implication. Standard notions of oxidation protection by means of a coating imply that the protector material is more passive in oxidation than the material being protected. That does not seem to be the case in this system. Consider the sample coated with Cu–21Cr, for instance, in Fig. 2. Its final weight gain at the end of the 20 h test was ~1.9 mg/cm^2, but 1.6 mg/cm^2 or 84% of that net weight gain occurred in the ~4 h before cross-over to the passive side of the substrate.

Taken together, these two points suggest that coatings with ≤26 wt.% Cr would not provide *passive* protection over a Cu–8Cr–4Nb liner's service life, which is the same conclusion reached by Chang et al. [7,8]. However, there is another sense in which a coating can protect a nobler substrate from environmental attack: by functioning as a sacrificial layer—a concept familiar from the galvanic protection of metal alloys from aqueous corrosion. As might be expected (since internal oxidation was not observed in this study) the coatings had to be consumed before oxidation of the substrate set in. Fig. 7(b) shows a situation in which the oxide interfaces with the substrate, indicating that the coating was all consumed; and Fig. 6(b) showed the consequence of that situation in terms of runaway cyclic oxidation. Time gained by the consumption of the coating amounts to "sacrificial" protection.

It was shown earlier that, for Cu–21Cr oxidized at 650 °C, 84% of the total weight gain occurred before the onset of parabolic kinetics. Cu–17Cr showed similar behavior, with the onset of parabolic behavior shifted to even longer times. This underscores the point that the first few hours of oxidation constitute the main stage in the degradation of these Cu–Cr coatings, and efforts to improve Cu–Cr protection must address ways to suppress oxidation in the first couple of hours. The results presented here indicate that one way to do this is to increase Cr content. However, if a coating must stay Cr-lean (to promote ductility and conductivity, as in thruster applications) a different solution must be found, and it has been suggested that a higher degree of textual and microstructural refinement in these coatings (perhaps down to nanometer scale) is the way to go [12]. It may also be the way to turn these alloys into exclusive Cr_2O_3 formers by suppressing Cu oxidation altogether, a situation observed in special cases by Niu et al. [11] but not in this study.

The oxide microstructures in Fig. 8 explain why these Cu–Cr alloys gain weight rapidly initially, only to slow down later to the passive side of the substrate. Note, in Fig. 8(a), that Cr_2O_3, the source of passive protection, nucleates as discrete and large islands; it is only with continued oxidation that the islands coalesce into a continuous diffusion barrier that suppresses oxidation by retarding oxygen diffusion. Comparison of Fig. 8(a) and (b) shows that Cr_2O_3 coalescence into a protective barrier occurs earlier in those alloys with higher Cr levels: For tests at the same temperature and of the same duration, a continuous Cr_2O_3 is formed earlier in the oxidation of Cu–21Cr than of Cu–17Cr. This agrees entirely with the weight gains in Fig. 2.

5. Summary and conclusion

Oxidation behavior of Cu–*x*Cr (*x*=17–26 wt.%) compositions has been evaluated by static and cyclic oxidation, both on stand-alone coupons and as coatings on Cu–8Cr–4Nb substrate, with emphasis on determining the range of compositions, temperatures and times for which the coating can protect the substrate. It was found that for static oxidation Cr contents above 8.5% can offer adequate protection up to 20 h and 750 °C; for cyclic oxidation Cr values of 21% and higher are needed for protection up to 10 h at 750 °C; Cu–17Cr may last 10 h only up to 650 °C, and less than 3 h at 750 °C. Thus, the higher the Cr content the greater the protection provided. But the protection achieved in the first few hours (which coincide with the probable life of a liner) is essentially by "sacrificial" rather than passive oxidation. Most weight gain of a coated sample occurs in that stage because the Cr_2O_3 sub-oxide layer is discontinuous, hence unable to function as an effective diffusion barrier. However, with increasing Cr content and higher oxidation temperature that vulnerable initial stage becomes shorter.

Acknowledgment

This work was performed at the NASA Glenn Research Center in Cleveland, Ohio, as part of the Next-Generation Launch Technology. It was funded under contract No. NAS3-00145.

References

[1] A. Ronnquist, H. Fischmeister, J. Inst. Met. 89 (1960–61) 65.
[2] J.H. Park, K. Natesan, Oxid. Met. 39 (5/6) (1993) 411.
[3] S. Mrowec, A. Stoklosa, Oxid. Met. 3 (3) (1971) 291.
[4] G.M. Reynaud, W.A.T. Clark, R.A. Rapp, Metall. Trans., A, Phys. Metall. Mater. Sci. 15A (1984 March) 573.
[5] L.U. Ogbuji, Mater. High Temp. 2 (2004) 101.
[6] J.R. Davis (Ed.), Copper and Copper Alloys, ASM International, Materials Park, OH, 2001, p. 372.
[7] K.T. Chiang, J.L. Yuen, Surf. Coat. Technol. 61 (1993) 20.
[8] K.T. Chiang, T.A. Wallace, R.K. Clark, Surf. Coat. Technol. 86–87 (1996) 48.
[9] R.J. Walker, K.T. Chiang, Mater. Sci. Eng., A Struct. Mater.: Prop. Microstruct. Process. 263 (1999) 8.
[10] Y. Niu, F. Gesmundo, F. Vianni, D.L. Douglass, Oxid. Met. 48 (5/6) (1997) 357.
[11] G.Y. Fu, Y. Niu, F. Gesmundo, Corros. Sci. 45 (2003) 559.
[12] L.U. Ogbuji, in: E. Lara-Curzio, M.J. Ready (Eds.), Ceramic Eng. and Sci. Proc., vol. 45, Nos. 3–4, Am. Ceram. Soc., Westerville, OH, 2004, pdf-159.

[13] F. Gesmundo, B. Gleeson, Oxid. Met. 44 (1/2) (1995) 211.
[14] M.P. Brady, P.F. Tortorelli, L.R. Walker, Mater. High Temp. 17 (2) (2000) 235.
[15] H. Gabel, R. Tapphorn, in: T.S. Sudarshan, W. Reitz, J.J. Steiglich (Eds.), Proc. TMS and ASM International: Surface Modification Technologies IX, TMS, Warrendale, PA, 1995.
[16] D.B. Morgan, et al., in: J. Richmond, S. Wu (Eds.), Advanced Earth-to-Orbit Propulsion Tech. 1988, NASA Conf. Publication 3012, vol. II, 1988.
[17] L.U. Ogbuji, D.L. Humphrey, Oxid. Met. 60 (3/4) (2003) 271.
[18] C.A. Barrett, C.E. Lowell, Oxid. Met. 11 (4) (1977) 199.
[19] L. Ogbuji, Oxid. Met. (in press).